IEEE Access
Multidisciplinary | Rapid Review | Open Access Journal

Received 13 December 2024, accepted 13 January 2025, date of publication 20 January 2025, date of current version 27 January 2025.

Digital Object Identifier 10.1109/ACCESS.2025.3531395

RESEARCH ARTICLE

Mitigation of Diffraction Effect in GNSS Positioning Considering Azimuth and PDOP in Canyon Environment

QINGFENG WU[1], (Graduate Student Member, IEEE), XIAOYA WANG[1,2,3], AND HOUXIANG ZHOU[4]

[1]Shanghai Astronomical Observatory, Chinese Academy of Sciences, Shanghai 200030, China
[2]School of Astronomy and Space Science, University of Chinese Academy of Sciences, Beijing 100049, China
[3]Shanghai Key Laboratory of Space Navigation and Positioning Techniques, Shanghai Astronomical Observatory, Chinese Academy of Sciences, Shanghai 200030, China
[4]College of Surveying and Geo-Informatics, Tongji University, Shanghai 200092, China

Corresponding author: Xiaoya Wang (wxy@shao.ac.cn)

This work was supported by the National Natural Science Foundation of China under Grant 12373076, and by Shanghai Key Laboratory of Space Navigation and Position Techniques under Grant 06DZ22101.

ABSTRACT Global navigation satellite system (GNSS) monitoring stations established in canyon environments inevitably face challenges such as multipath effects, diffracted signals, and non-line-of-sight (NLOS) reception due to obstructions. To address this problem, existing methods employ a stochastic model based on GNSS receiver signal-to-noise ratio (SNR) to detect NLOS reception. However, the method only accounts for NLOS reception concerning elevation angles of satellites, neglecting NLOS reception from obstructions at side edges. To overcome this limitation, this paper proposes a threshold of azimuth angle. When the threshold is considered, it does not only improve NLOS detection, but also increases the position dilution of precision (PDOP) value, potentially affecting positioning precision. Thus, we introduced a PDOP stochastic model and proposed a method that integrates both the azimuth angle threshold and PDOP considerations. Experimental results show that the precision of the stochastic model based on equivalent elevation angles improves by approximately 24.25% after considering the threshold of azimuth angle. Furthermore, the precision increases by an additional 8.69% when the PDOP stochastic model is also taken into account.

INDEX TERMS Canyon environment, equivalent elevation, non-line-of-sight (NLOS) reception, position dilution of precision (PDOP) stochastic model.

I. INTRODUCTION

The Global Navigation Satellite System (GNSS) has been widely utilized in high-precision ground deformation detection, subsidence monitoring, geoscientific research, and structural health monitoring such as landslides, dams, or bridges [1], [2], [3]. The continuously operating reference station (CORS) plays a crucial role in the application of GNSS [4]. One of the key functions of CORS is to provide real-time, continuous GNSS observation data for relative positioning [4], [5]. With the introduction of the concept of CORS, many cities have established their own CORS systems, even located CORS stations in urban environments [6], [7]. However, the use of GNSS receivers in urban environments faces significant challenges. The primary issues stem from non-line-of-sight (NLOS) reception caused by urban structures in canyon environments, which induce multipath effects, signal blockage, and diffraction of navigation satellite signals [8], [9], [10]. These factors substantially deteriorate the service performance of urban CORS stations, thereby reducing positioning precision.

The associate editor coordinating the review of this manuscript and approving it for publication was Venkata Ratnam Devanaboyina.

Accurate NLOS detection and subsequent processing are essential to signal quality control [11], [12]. SNR is a main indicator that reflects the signal quality due to the relationship between SNR and signal quality [13], [14]. The exponential function of SNR with base 10 is a famous and popular stochastic model served as a weighting scheme of GNSS observations, especially in a low signal quality scenario [15], [16], [17]. However, traditional stochastic models such as the exponential function of SNR with base 10 cannot reasonably estimate the accuracy of different types of satellite measurements at a specific site [18]. To address the challenges caused by NLOS in canyon environments, Strode and Groves in 2015 proposed a method for detecting multipath effects using the tri-frequency SNR observations [19]. The method involves first establishing an SNR-based multipath detector between the SNR observations at different frequencies and satellite elevation angles under low NLOS conditions [19]. The observed SNR is then compared against the detector to detect the multipath even diffraction [19]. Based on Strode and Groves' method, Zhang et al. developed a technique for detecting multipath effects using dual-frequency SNR [20]. However, Špánik et al. pointed out several issues in 2018 [21]. First, whether the cubic polynomial used by Špánik et al. to establish the reference function can be applied to a broader range of scenarios requires further investigation [21]. Second, the validity of using a cubic polynomial to fit the relationship between SNR observations and elevation angles for establishing the reference function is questionable [21]. Third, while the reference function can accurately detect multipath effects in tri-frequency receivers, it may lead to erroneous detection in dual-frequency receivers [21].

To address these issues, Špánik et al. proposed the optimal combination estimator, which detects multipath effects by constructing a linear combination of SNR observations at multiple frequencies with the cosine of the elevation angle [21]. However, this method is only applicable to dual- or tri-frequency receivers. Although low-cost single-frequency receivers are more sensitive to NLOS reception, they have become more popular in the market because of their cheapness and portability [22], [43]. In 2021, Zhang et al. introduced a composite stochastic model designed for canyon environments. It proposed the concept of equivalent elevation angle and extended its applicability to single-frequency receivers [14]. While it is effective in detecting signal diffraction and multipath effects, this method only constrains the elevation angle using the azimuth angle of buildings. As a result, the azimuth angle does not directly limit satellite signals, thereby not fully utilizing its potential. In reality, NLOS effects of satellite signals can occur not only in the elevation direction of obstructions but also along the side edges of obstructions, particularly in the case of signal diffraction effects [24].

Another challenge in canyon environments is the reduction in the number of satellites and the increase in position dilution of precision (PDOP) due to obstruction by terrain features [25]. The number of satellites determines the amount of available observations, while PDOP reflects the strength of the geometric configuration between satellites [23]. An increase in PDOP leads to a decrease in positioning precision under the condition of having the same number of satellites, particularly when an angle threshold is used to exclude satellites in order to mitigate NLOS reception [26]. To minimize the impact of poor PDOP conditions in such challenging environments, Li et al. proposed a PDOP considering stochastic model in 2022, achieving approximately a 10% improvement in precision for single point positioning (SPP) [25]. However, research on PDOP considering stochastic models remains limited and is primarily applied to SPP [25], [27]. We propose employing a PDOP stochastic model to compensate for the drawbacks associated with increased PDOP due to the exclusion of satellites.

Canyon environments present complex influencing factors. Previous research has mostly used azimuth angles as constraints on elevation angles, indirectly affecting satellite selection. Therefore, this study considers the potential for satellite signal NLOS reception at the side edges of obstructions and proposes using satellite azimuth angles as direct constraints to control satellite selection. Its main contributions are as follows: First, we introduce an azimuth threshold method, considering the NLOS reception of satellite signals at the side edges of obstructions. Second, due to the exclusion of some satellites using the elevation and azimuth angle filtering mechanism, leading to an increase in PDOP, we incorporate a PDOP stochastic model to mitigate its impact on positioning precision. Third, we reevaluate the classification strategy of the template function, establishing different template functions for different types of satellites within the same receiver. Section II provides a detailed introduction to this method and strategy. Subsequently, Section III verifies the proposed method using a geodetic receiver. The conclusions are presented in Section IV.

II. METHOD

In this section, we first introduce the weighted method for equivalent elevation angles and the PDOP stochastic model. Then, we present the concept of azimuth angle threshold, followed by a new template function classification strategy.

A. EQUIVALENT ELEVATION STOCHASTIC MODEL

The elevation-dependent stochastic model is a commonly used method for assigning weights to navigation satellite observations. It involves assigning different weights to each observation based on the elevation angle of the satellite to the receiver at the current epoch. The stochastic model expression is given as follows [29], [30]:

$$\sigma = \frac{a}{\sin^2(\theta)} \tag{1}$$

where σ represents the precision of undifferenced and uncombined GNSS observations, a is a constant coefficient, and θ denotes the elevation angle of the observed satellite.

In general, to minimize the impact of multipath effects from low-elevation satellites and diffracted signals from satellites below the horizon, GNSS data processing typically involves applying a constant natural cut-off elevation angle [14]. However, in canyon environments, especially in urban canyons, obstructions can also obscure GNSS signals, cause multipath effects and diffraction, and then affect the GNSS receiver [14], [21]. Therefore, obstructions could be treated as part of the horizon in such scenarios. From the receiver's perspective, the elevation angle of the obstruction is correlated with its azimuth angle. Consequently, it is necessary to establish the relationship between the elevation and azimuth angles of the obstructions, where the elevation angle is referred to as the geographic elevation angle, and the natural cut-off elevation angle is subsequently added [14], [41]. The expression is as follows [14]:

$$\tau' = \tau + \theta_{geo}\left(\omega_r^s\right), \quad \omega_r^s \in [0, 2\pi] \tag{2}$$

where ω_r^s represents the azimuth angle of the satellite s in the local coordinate system of the receiver r, $\theta_{geo}\left(\omega_r^s\right)$ denotes the geographic cut-off elevation angle, which is a function of the satellite's azimuth angle ω_r^s for a certain site, and τ' refers to the cut-off elevation angle of the satellite, considering the impact of obstructions. In addition, the expression of $\theta_{geo}\left(\omega_r^s\right)$ implicates the boundary of the obstructions around the receiver. Therefore, the expression of $\theta_{geo}\left(\omega_r^s\right)$ should be formulated based on the environment surrounding the receiver.

The elevation angle of a satellite to an obstruction is referred to as the constrained elevation angle, and its expression is as follows [14]:

$$\bar{\theta}_{r,i}^s = \theta_{r,i}^s - \theta_{geo}\left(\omega_r^s\right) \tag{3}$$

where $\bar{\theta}_{r,i}^s$ represents the constrained elevation angle of satellite s to receiver r at signal frequency i, and $\theta_{r,i}^s$ is the elevation angle of satellite s to receiver r at signal frequency i. Similar to the requirement that the satellite's elevation angle must exceed the natural cut-off elevation angle, the constrained elevation angle must also be greater than the cut-off elevation angle τ.

After obtaining the constrained elevation angle, it is necessary to evaluate and adjust it using the SNR to derive the final equivalent elevation angle [14]. The basis for this evaluation is the template function. A template function is an SNR-elevation angle relationship established for a specific receiver in a low NLOS environment [14], [20]. It also involves calculating the standard deviation (STD) of the SNR observations relative to this function, where the STD is also a function of the elevation angle. The SNR-elevation angle function and the STD-elevation angle function together form the template function [14]. Zhang et al. used cubic polynomials to fit the SNR observations and STD to obtain the following template function [14], [20]:

$$SNR^*\left(\theta_{r,i}^s\right) = \alpha_1 + \alpha_2 \times \theta_{r,i}^s + \alpha_3 \times \left(\theta_{r,i}^s\right)^2 + \alpha_4 \times \left(\theta_{r,i}^s\right)^3 \tag{4}$$

$$STD^*\left(\theta_{r,i}^s\right) = \beta_1 + \beta_2 \times \theta_{r,i}^s + \beta_3 \times \left(\theta_{r,i}^s\right)^2 + \beta_4 \times \left(\theta_{r,i}^s\right)^3 \tag{5}$$

where $SNR^*(\theta_{r,i}^s)$ and $STD^*(\theta_{r,i}^s)$ are the template SNR and its corresponding STD for the elevation angle $\theta_{r,i}^s$ and $\alpha_i\,(i = 1, 2, 3, 4)$ and $\beta_i\,(i = 1, 2, 3, 4)$ are the fitting coefficients of the cubic polynomials for the template SNR and its STD, respectively [14].

After obtaining the template function, it can be used as prior information to detect NLOS reception in satellite signals received by GNSS receivers in canyon environments and to determine the corresponding equivalent elevation angles. If the observed SNR in the canyon environment satisfies the following condition [14]:

$$\left|SNR\left(\bar{\theta}_{r,i}^s\right) - SNR^*\left(\bar{\theta}_{r,i}^s\right)\right| \le k \cdot STD^*\left(\bar{\theta}_{r,i}^s\right) \tag{6}$$

where k represents the multiple of the standard deviation, taking values of 1, 2, or 3, then the equivalent elevation angle can be taken as the constrained elevation angle. Otherwise, the constrained elevation angle must be adjusted as follows [14]:

$$\begin{cases} \bar{\theta}_{r,i}^s = \bar{\theta}_{r,i}^s - \delta, & SNR\left(\bar{\theta}_{r,i}^s\right) \le SNR^*\left(\bar{\theta}_{r,i}^s\right) \\ \bar{\theta}_{r,i}^s = \bar{\theta}_{r,i}^s + \delta, & SNR\left(\bar{\theta}_{r,i}^s\right) > SNR^*\left(\bar{\theta}_{r,i}^s\right) \end{cases} \tag{7}$$

where δ is the adjustment constant determined by the resolution of the template function. This adjustment process is repeated until the condition in (6) is satisfied, yielding the final equivalent elevation angle. If the adjustment reaches the minimum elevation angle τ or the maximum angle of 90° without satisfying the condition in (7), then the equivalent elevation angle is set to either this minimum or maximum value. The final equivalent elevation angle is then used as the input variable for the elevation angle stochastic model, and the weight for each satellite's signal at different frequencies is determined by (1) [14].

B. STOCHASTIC MODELING CONSIDERING THE PDOP

A key method of the PDOP stochastic model is to increase the weight of critical satellites, which are defined as those that significantly contribute to the PDOP value. First, the base function of PDOP must be calculated [25]:

$$f(PDOP) = \begin{cases} \dfrac{1}{k_i^\beta}, & k_i^\beta \le \gamma \\ \dfrac{1}{\gamma}, & k_i^\beta > \gamma \end{cases} \tag{8}$$

where β is an adjustment parameter that can be set between 1 and 3 based on specific conditions, and γ is a threshold set to prevent excessive amplification, k_i represents the contribution of satellite i to PDOP, it can be calculated as

follows [25]:

$$k_i = \frac{PDOP_i}{PDOP_{all}} \tag{9}$$

where $PDOP_i$ represents the PDOP value after excluding satellite i, and $PDOP_{all}$ is the PDOP value determined by all available satellites.

The calculation of PDOP requires the covariance matrix of the parameters to be estimated, and is given by the following formula [31], [39]:

$$PDOP = \sqrt{Q_{XX} + Q_{YY} + Q_{ZZ}} \tag{10}$$

where the different subscripts of Q represent the variances of the three coordinate parameters.

The stochastic model that accounts for PDOP is then expressed as [25]:

$$\sigma^2_{PDOP} = f(PDOP) \times \sigma^2 \tag{11}$$

where σ^2_{PDOP} represents the observation precision considering PDOP, and σ^2 is the observation precision without PDOP consideration. The value of σ^2 can be obtained using the elevation weighting method through (1) after calculating the equivalent elevation angle.

C. AZIMUTH THRESHOLD

In GNSS positioning, it is necessary to establish a natural cut-off elevation angle as the minimum elevation angle for all navigation satellites [14]. Satellites with elevation angles below this threshold should be excluded [41]. Due to signal diffraction and atmospheric refraction, some navigation satellite signals below the horizon may still be received by GNSS receivers, leading to observations with significant errors and then reducing positioning precision. In canyon environments, the upper edges of obstructions within the canyon effectively become the new horizon, making the cut-off elevation angle equal to τ' as defined in (2).

However, the scenario of obstructions in canyon environments is more complex. Fig. 1. illustrates the faulty observations caused by diffraction signals from the upper and side edges of obstructions. Particularly in cases where there is a significant height difference among multiple obstructions, the diffraction signals from the side edges of the obstructions need to be handled appropriately. Therefore, we consider the method of setting an azimuth angle threshold for navigation satellite signals in canyon environments. It is important to note that, unlike the cut-off elevation angle, an obstruction has two sides rather than just one. Thus, the threshold needs to account for both the left and right directions:

$$\begin{cases} \alpha_{left} = \omega^-_{obstruction} - m \\ \alpha_{right} = \omega^+_{obstruction} + m \end{cases} \tag{12}$$

where α_{left} and α_{right} represent the left and right azimuth angle limits relative to the obstruction as seen by the receiver, $\omega^-_{obstruction}$ and $\omega^+_{obstruction}$ are the azimuth angles of the left and right edges of the obstruction, respectively, and m denotes the threshold. If a satellite's azimuth angle ω satisfies:

$$\alpha_{left} < \omega < \alpha_{right} \tag{13}$$

then the satellite should be excluded.

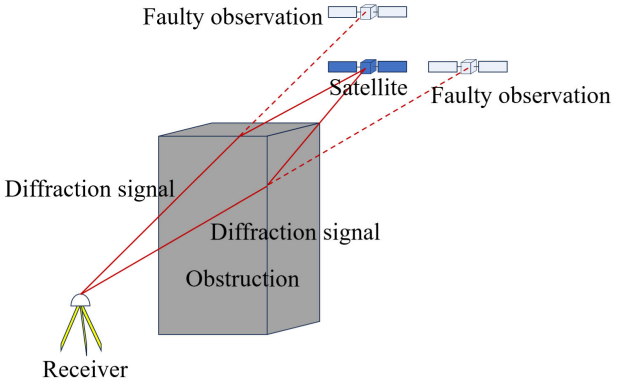

FIGURE 1. Diffraction signals can cause faulty observations of satellites by GNSS receivers. The diagram illustrates the impact of diffraction signals from the upper and side edges of the obstruction on observation.

However, setting an azimuth angle threshold may lead to an increase in PDOP, thereby deteriorating positioning precision due to the exclusion of satellites. Conversely, if the azimuth angle threshold is not applied, the PDOP stochastic model might increase the weight of satellites affected by diffraction signals, which can also negatively impact positioning precision. Therefore, the use of an azimuth angle threshold and a PDOP stochastic model may complement each other, and it is advisable to employ both methods simultaneously.

D. THE CLASSIFICATION OF TEMPLATE FUNCTION

In template function determination, it should be considered by different navigation constellations separately. Even within the same navigation constellation, variations in antenna types of satellites necessitate distinct template functions for different satellites [14]. For example, in the study by Zhang et al., it was noted that within the GPS constellation, the SNR on the L2 frequency differs between Block IIR and other satellite types, leading to a distinction in template functions based on whether a satellite is a Block IIR type or not.

We have adopted and further developed this strategy. For the GPS constellation, it was observed that the L2 signal cannot be simply differentiated based on whether the satellite is a Block IIR type, as the SNR-elevation angle distribution exhibited multiple distinct trends. This implies that template functions should be established for various types of GPS satellites, likely due to advancements in satellite technology. We classified the GPS satellites into four categories: Block IIR, Block IIR-M, Block IIF, and Block III [32]. For the Galileo constellation, satellites are categorized into two types: In-Orbit Validation (IOV) satellites and Full Operational Capability (FOC) satellites [33], [34]. Currently,

FIGURE 2. The size of the obstruction (left panel) and the relationship of the obstruction (right panel) [36]. In the left panel, the yellow point notifies the receiver. And the azimuth of the center of the obstruction is 330°. We assume the obstruction is a sphere. According to the measurement tools, the diameter of the sphere is about 14 m, and the horizontal distance from the center of the sphere to the receiver is about 10 m, the height difference between the top of the sphere and the receiver is about 11 m.

there are three IOV satellites in orbit with pseudo random noise(PRN) codes E11, E12, and E19, while the rest are FOC satellites. We observed that template functions for IOV and FOC satellites differ for both the E1 and E5b frequencies. Therefore, it is necessary to establish separate template functions for IOV and FOC satellites for the E1 and E5b frequencies in the Galileo system.

III. EXPERIMENT

This experiment requires conducting measurements in an environment with signal obstructions. We selected the Tate's Cairn station (TCHK) of the Hong Kong Satellite Positioning Reference Station Network (SatRef) for the experiment. This station is part of the Hong Kong CORS network and utilizes a Trimble Alloy receiver with a Leica AR25.R4 antenna. It is located adjacent to the Tate's Cairn Meteorological Station Hong Kong Observatory, as illustrated in Fig. 2.

Firstly, we need to establish a function expression for the geographic elevation angle based on the buildings near the TCHK station. Information about the obstructions around the TCHK station can be obtained from the three-dimensional digital map publicly released by the Hong Kong Lands Department. The three-dimensional map indicates that the only obstruction near the TCHK station is a spherical building, while other directions offer an open view. Details of the spherical building are shown in Fig. 2. We assume this spherical building is the sole obstruction and is a regular sphere. When the line of sight from the receiver to the satellite is tangent to the sphere, it is considered the boundary of the obstructed region. Based on geometric relationships, the distance r from the receiver to the points on the boundary of the obstructed region can be determined as:

$$r = \sqrt{H^2 + D^2 - R^2} \tag{14}$$

where H is the height difference between the spherical center and the receiver, D is the horizontal distance between the spherical center and the receiver, R is the radius of the sphere. Based on the information in Fig.2., the spherical coordinate

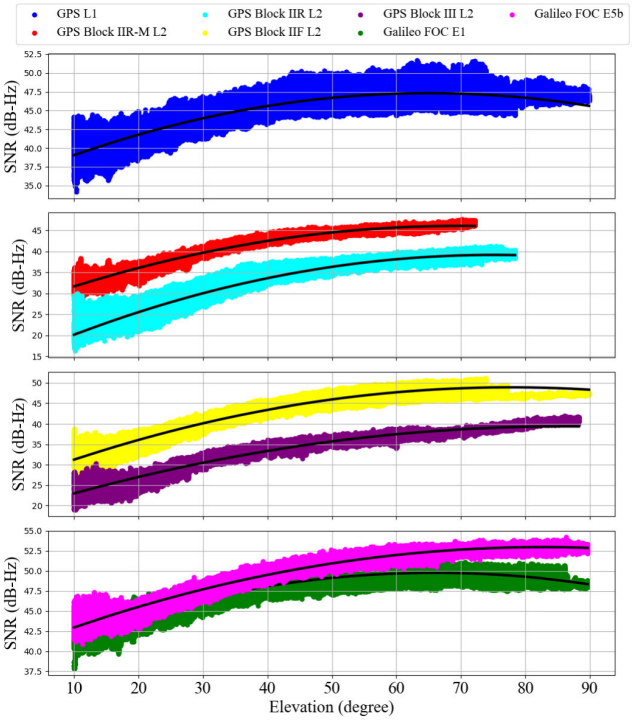

FIGURE 3. The relationship between SNR observations collected in a low-NLOS environment and elevation angle. The black curve represents the cubic polynomial fitting function.

expression of the sphere can be obtained in a coordinate system centered at the receiver. Incorporate (14) into the spherical coordinate expression of the sphere, the equation of the obstructed region boundary $f(\theta, \omega)$ can be expressed as follows:

$$f(\theta, \omega) = \frac{H^2 + D^2 - R^2}{(D \cdot \cos\theta \cdot \cos(\omega - \omega_0) + H \cdot \sin\theta)^2} - 1 \tag{15}$$

where θ is the elevation angle of the building, ω is the azimuth angle of the building, and ω_0 is the azimuth angle of the building's center. The equation $f(\theta, \omega) = 0$ represents the boundary of the building from the receiver's perspective. If $f(\theta, \omega) < 0$, it indicates that the satellite located at (θ, ω) is within the obstructed region.

A. DETERMINATION OF TEMPLATE FUNCTIONS

After confirming the type of receiver and antenna, it is essential to establish the template function for the specific receiver and antenna configuration. The determination of the template function requires the collection of SNR observational data in a low-NLOS environment. For this purpose, we used the IGS station CEDU00AUS located in Ceduna, Australia, which is equipped with the same Trimble Alloy receiver and Leica AR25.R4 antenna. SNR observations were collected over a 24-hour period on the day of year 183 in 2024, with a sampling interval of 1 second. The data includes observations for the GPS L1 (1572.42 MHz) and L2 (1227.60 MHz) frequencies, as well as the Galileo E1

TABLE 1. The coefficients of SNR and STD template functions.

Classification	α_1	α_2	α_3	α_4	β_1	β_2	β_3	β_4
GPS L1	35.694	0.362	2.943×10^{-3}	1.650×10^{-6}	2.528	-0.125	2.853×10^{-3}	-1.937×10^{-5}
GPS Block IIR L2	15.667	0.493	4.913×10^{-4}	-3.958×10^{-5}	2.771	-0.075	1.108×10^{-3}	-6.542×10^{-6}
GPS Block IIR-M L2	28.193	0.377	1.387×10^{-3}	-4.629×10^{-5}	2.374	-0.107	1.944×10^{-3}	-1.165×10^{-5}
GPS Block IIF L2	27.791	0.396	1.397×10^{-3}	-3.977×10^{-5}	2.867	-0.139	3.089×10^{-3}	-2.154×10^{-5}
GPS Block III L2	17.015	0.618	-6.119×10^{-3}	2.404×10^{-5}	2.604	-0.107	1.863×10^{-3}	-1.0920×10^{-5}
Galileo FOC E1	39.502	0.277	-1.219×10^{-3}	-9.247×10^{-6}	1.835	-0.085	1.854×10^{-3}	-1.232×10^{-5}
Galileo FOC E5b	41.188	0.202	-9.095×10^{-4}	-2.055×10^{-5}	1.417	-0.060	1.081×10^{-3}	-6.404×10^{-6}

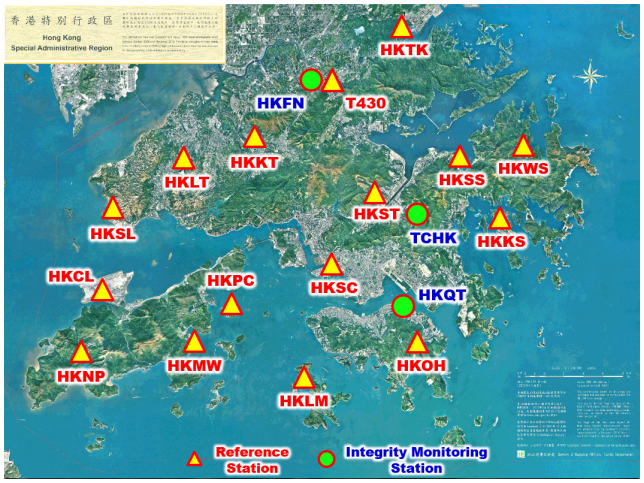

FIGURE 4. The CORS stations of SatRef [37].

(1572.42 MHz) and E5b (1207.14 MHz) frequencies. Based on the classification principles for template functions, we also apply the least squares method to fit the data in the low-NLOS environment using cubic polynomials, thereby obtaining the fitting coefficients [14]. The coefficients of (4) and (5) are outlined in Table 1.

The reason for not determining template functions for the IOV satellites in the Galileo constellation is that there are only three IOV satellites, and their template functions are not consistent. The impact of excluding IOV satellites on positioning results is minimal, therefore, this study does not consider them. Fig. 3. presents the SNR observations in a low-NLOS environment and the template functions for various types of satellites within the GPS and Galileo constellations. It can be observed that, for the GPS L1 signal, all satellites exhibit the same trend in the SNR-elevation relationship. However, for the L2 signal, the trend varies according to satellite type. Specifically, the satellites categorized as Block IIR, Block IIR-M, Block IIF, and Block III each demonstrate different trends, indicating the need for distinct template functions. Similarly, Galileo's FOC satellites require separate template functions for the E1 and E5b signals.

B. ANALYSIS OF POSITIONING PERFORMANCE

We analyzed 20 hours of data collected from the TCHK station on the day of year 183 in 2024, spanning from

TABLE 2. Processing strategy.

Items	Description
Positioning mode	RTK
TCHK coordinates (m)	(-2421068.4081, 5382639.8524, 2411312.1769)
HKST coordinates (m)	(-2417143.6676, 5382345.2053, 2415036.6620)
Baseline	5.419 km
Used signals	GPS L1, GPS L2, Galileo E1 and Galileo E5b
Natural cut-off elevation	10°
Azimuth threshold	10°
Ambiguity resolution	LAMBDA, partial ambiguity resolution
Ionospheric correction	Single layer model
Tropospheric correction	Niell mapping function and global mapping function
Ratio value	2.0

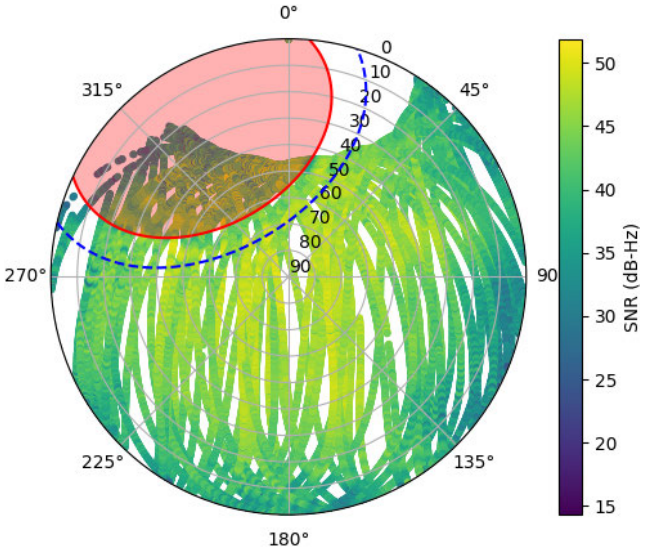

FIGURE 5. Sky plot of the TCHK station. The red shaded area indicates the range of the building, while the blue dashed line represents the boundary considering both the cut-off elevation angle and azimuth angle threshold.

02:00:00 to 22:00:00, with a sampling interval of 30 seconds. Fig. 6. is the map of SatRef. The processing strategy for the experiment is outlined in Table 2. Real-time kinematic (RTK) mode is used to validate the methods, as TCHK is set to the static rover and HKST is set to the base station. The reference coordinates of the two stations are determined by precise point positioning (PPP) in the earth-centered, earth-fixed (ECEF) coordinate system. The least squares ambiguity decorrelation adjustment (LAMBDA) method is used to fix the integer ambiguity [40]. For partial ambiguity resolution,

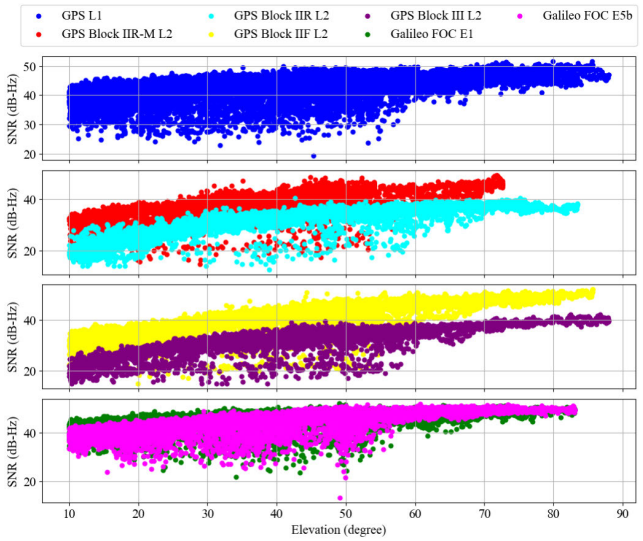

FIGURE 6. Distribution of SNR with elevation angle in the presence of building obstructions. The legend is the same as in Fig. 3.

TABLE 3. Accuracy statistics with methods ELEM, COPM, COAM and CAPM.

	ELEM	COPM	DOPM	COAM	CAPM
East error (mm)	12.160	1.995	2.288	2.508	2.661
Norht error (mm)	6.359	6.018	6.916	5.887	5.919
Up error (mm)	17.854	12.096	15.007	8.128	6.863
Ambiguity fixing rates (%)	20.5	90.7	90.2	95.5	95.5

a straightforward elevation angle selection criterion was employed, fixing the integer ambiguity only when the satellite's elevation angle exceeded 35°. The elevation angle resolution for the STD calculation was set to 0.01°. In the elevation-dependent stochastic model, the parameter a was set to 0.005 as it yielded the best performance in a series of experiments by using the elevation-dependent stochastic model alone. In (6), the value of k was set to 3, in (7), δ was set to 1, and in (8), β was set to 2, γ set to 10 [14], [25].

The relationship between the satellite sky plot and the building is illustrated in Fig. 5. It is evident that the SNR of satellite signals within the shaded area is significantly weaker and less stable compared to other regions at the same elevation angle. Additionally, SNR instability is observed even outside the shaded area but within the blue dashed lines. It indicates the presence of NLOS reception near the building and its boundaries.

The observed SNR-elevation angle distribution at the TCHK station is depicted in Fig. 6. Due to the presence of NLOS reception caused by building obstructions, significant fluctuations in SNR are evident, markedly different from the SNR-elevation angle distribution under low-NLOS conditions. This irregularity is particularly pronounced at elevation angles below 60°. Moreover, in the Galileo system, even at higher elevation angles, the SNR distribution of E1 and E5b signals, which are expected to exhibit distinct trends, unexpectedly converge. Therefore, the determination of template functions based on SNR observations in low-NLOS environments is of great significance for correcting NLOS reception in obstructed situations.

To evaluate the effectiveness of the proposed method, we conducted a comparative analysis of several established methods: the traditional elevation-dependent stochastic model (ELEM), which weights satellites by elevation angles based on (1) alone; Zhang et al.'s equivalent elevation angle stochastic model (COPM), described in Section II-A as an extension of ELEM, which aims to improve satellite selection and weighting by using an equivalent elevation angle approach; the COPM incorporating the PDOP statistic model(DOPM); the COPM incorporating the proposed azimuth angle threshold method (COAM), which introduces an azimuth angle constraint to enhance model robustness in challenging environments; and the method combining the azimuth angle threshold with a PDOP stochastic model (CAPM), which further improves positioning accuracy by considering the impact of PDOP. These five methods were evaluated to assess the effectiveness of the proposed method, focusing on the impact of the azimuth angle threshold and the precision improvements with the PDOP stochastic model. Fig. 7. and Table 3 shows the comparison of positioning accuracy obtained by the proposed and previous methods.

The root mean square errors (RMSE) in the three-dimensional directions for the CAPM, COAM, DOPM, COPM, and ELEM methods are 9.445 mm, 10.345 mm, 16.682 mm, 13.657 mm, and 22.518 mm, respectively. The ambiguity fixing rates of COPM, DOPM, COAM, and CAPM are significantly higher than the traditional method ELEM. These indicate that the combined consideration of azimuth, elevation angle, SNR, and PDOP provides a significant improvement over the traditional method that only considers elevation angle. Specifically, COPM improves three-dimensional precision by approximately 39.35% compared to ELEM, which is consistent with the results of Zhang et al. [14], highlighting the effectiveness of the COPM method.

Following the implementation of the azimuth angle threshold, it is evident that COAM improves positioning precision compared to COPM, suggesting that setting an azimuth angle threshold can reduce the impact of NLOS reception from nearby obstructions, thereby enhancing precision by about 24.25%. A comparison between CAPM and COAM shows that, after minimizing NLOS reception, the PDOP stochastic model can adjust the weights of existing satellites to mitigate the higher PDOP values caused by satellite exclusion, thereby improving positioning precision by approximately 8.69%.

The DOPM method, as a COPM method incorporating the PDOP stochastic model, exhibits worse positioning accuracy compared to COPM. However, after incorporating the azimuth angle threshold, positioning accuracy improved, it demonstrates the importance of using the azimuth angle threshold to exclude faulty observations. In others words,

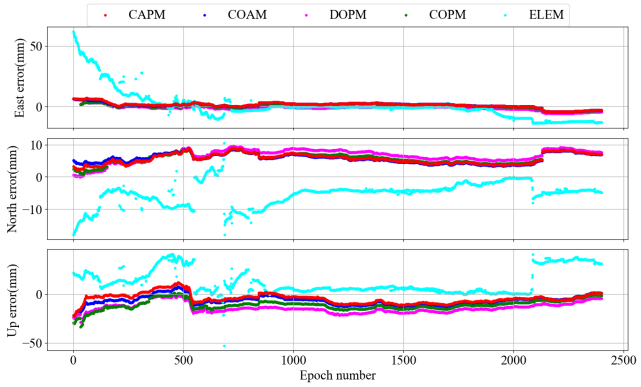

FIGURE 7. The distribution of positioning errors in the local coordinate system for CAPM, COAM, DOPM, COPM, and ELEM methods. Thex-axis represents the epoch ordinal number. Red points denote positioning errors for CAPM, blue points indicate errors for COAM, magenta points represent errors for DOPM, green points represent errors for COPM, and cyan points show errors for ELEM.

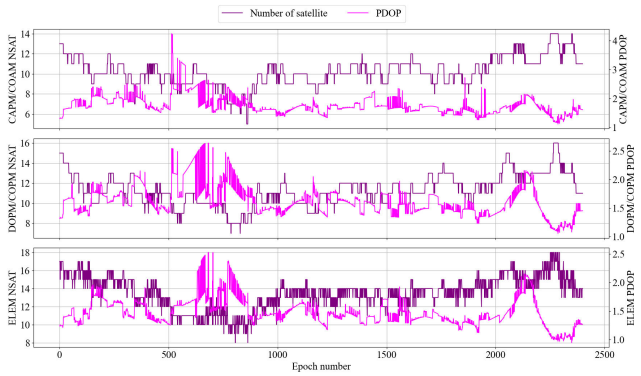

FIGURE 8. The distribution of satellite count (NSAT) and PDOP values. The panels are arranged from top to bottom corresponding to the CAPM/COAM, DOPM/COPM, and ELEM methods. Purple represents NSAT, and magenta represents PDOP values. CAPM and COAM share the same NSAT and PDOP values, hence they are displayed in the same panel.

a statistic model should be applied after faulty observations have been effectively eliminated.

Using the GPS G11 satellite as an example, Fig 9. illustrates the distribution of carrier-phase double-difference (DD) residuals for this satellite. A DD residual of zero indicates that the satellite is serving as the reference satellite for the current epoch. The RMSE of DD residuals for the CAPM, COAM, DOPM, COPM, and ELEM methods are 1.893 cm, 1.929 cm, 2.541 cm, 2.597 cm, and 4.420 cm, respectively. The ELEM method shows larger DD residuals, particularly in regions with obstructing structures, where DD residuals exceed 25 cm. This is due to the receiver primarily capturing diffracted signals from the satellite, leading to significant observation errors. Due to the PDOP statistic model, the DOPM shows smaller DD residuals compared with the COPM. This demonstrates the role of the stochastic model in improving internal consistency. Both COAM and CAPM methods address NLOS reception from satellites adjacent to obstructions by excluding those with

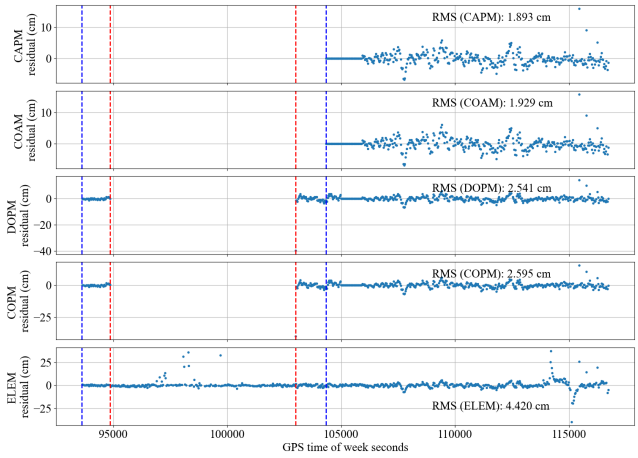

FIGURE 9. The distribution of carrier-phase DD residuals for the G11 satellite. The residuals are presented from top to bottom for the CAPM, COAM, DOPM, COPM, and ELEM methods. The red dashed lines on the left indicate the moments when the satellite crosses the boundary of the obstruction and its cut-off elevation angle, while those on the right mark the moments when the satellite exits these boundaries. The blue dashed lines on the left denote the times when the satellite enters the boundaries of the cut-off elevation and azimuth angles of the obstruction, with the lines on the right indicating when the satellite exits these boundaries.

large residuals in the azimuth angle threshold phase, resulting in lower DD residuals compared to the COPM method. The DD residuals for CAPM are lower than those for COAM, though the difference is not substantial.

IV. CONCLUSION

We have explored methods to mitigate the effects of NLOS reception by GNSS receivers in canyon environments. First, an equivalent elevation stochastic model based on template function which was appropriately classified by considering satellite types in different constellations was utilized. Then, a threshold of azimuth angle was used to exclude satellites around edges of obstructions where NLOS reception such as reflection and diffraction could occur. Finally, a stochastic model considering PDOP was used to mitigate the PDOP effect after excluding satellites.

Short baseline RTK experiments demonstrate that the use of the equivalent elevation angle stochastic model is effective in environments with NLOS reception, compared to the elevation-dependent stochastic model. The RMSE of positioning was 13.657 mm, representing a precision improvement of approximately 8.861 mm. When an azimuth angle threshold was applied to the equivalent elevation angle stochastic model, the RMSE of positioning decreased to 10.345 mm, resulting in a precision improvement of about 3.312 mm compared to when no azimuth angle threshold was used. Further, incorporating a PDOP stochastic model to mitigate the effects of PDOP on positioning precision, the RMSE of positioning reduced to 9.445 mm, which improved the positioning precision by approximately 0.9 mm. This represents the first application of the PDOP stochastic model in RTK positioning scenarios. The controlled experiments demonstrate that before applying the PDOP stochastic model,

faulty observations should be effectively eliminated, for instance, by employing the azimuth angle threshold method proposed in this study.

ACKNOWLEDGMENT

The authors would like to express their sincere gratitude to Li, Senior Land Surveyor with the Geodetic Survey Section, Survey and Mapping Office, Lands Department, Hong Kong, for providing the observation data used in this study. They also extend their thanks to the Geodetic Survey Section for making their data publicly available, which greatly facilitated their research.

REFERENCES

[1] X. Meng, A. H. Dodson, and G. W. Roberts, "Detecting bridge dynamics with GPS and triaxial accelerometers," *Eng. Struct.*, vol. 29, no. 11, pp. 3178–3184, Nov. 2007.

[2] P. Psimoulis, S. Pytharouli, D. Karambalis, and S. Stiros, "Potential of global positioning system (GPS) to measure frequencies of oscillations of engineering structures," *J. Sound Vib.*, vol. 318, no. 3, pp. 606–623, Dec. 2008.

[3] N. Liu, W. Dai, R. Santerre, J. Hu, Q. Shi, and C. Yang, "High spatio-temporal resolution deformation time series with the fusion of InSAR and GNSS data using spatio-temporal random effect model," *IEEE Trans. Geosci. Remote Sens.*, vol. 57, no. 1, pp. 364–380, Jan. 2019.

[4] W. A. Stone. *An Overview of Global Positioning System Continuously Operating Reference Stations*. NOAA. Accessed: Sep. 20, 2021. [Online]. Available: https://www.ngs.noaa.gov/PUBS_LIB/GPS_CORS

[5] R. A. Snay and T. Soler, "Continuously operating reference station (CORS): History, applications, and future enhancements," *J. Surv. Eng.*, vol. 134, no. 4, pp. 95–104, Nov. 2008.

[6] J. Liu, H. Liu, R. Zou, and N. Wei, "Some thoughts on the establishment of nationwide continuously operating reference stations," *Geomatics Inf. Sci. Wuhan Univ.*, vol. 34, no. 11, pp. 1261–1265, Nov. 2009.

[7] L. Yang, G. Wang, Y. Bao, T. J. Kearns, and J. Yu, "Comparisons of ground-based and building-based CORS: A case study in the region of Puerto Rico and the Virgin Islands," *J. Surv. Eng.*, vol. 142, no. 3, Aug. 2016, Art. no. 05015006.

[8] L.-T. Hsu, S.-S. Jan, P. D. Groves, and N. Kubo, "Multipath mitigation and NLOS detection using vector tracking in urban environments," *GPS Solutions*, vol. 19, no. 2, pp. 249–262, Apr. 2015.

[9] D. Dong, M. Wang, W. Chen, Z. Zeng, L. Song, Q. Zhang, M. Cai, Y. Cheng, and J. Lv, "Mitigation of multipath effect in GNSS short baseline positioning by the multipath hemispherical map," *J. Geodesy*, vol. 90, no. 3, pp. 255–262, Mar. 2016.

[10] J. Han, R. Tu, R. Zhang, L. Fan, and P. Zhang, "SNR-dependent environmental model: Application in real-time GNSS landslide monitoring," *Sensors*, vol. 19, no. 22, p. 5017, Nov. 2019.

[11] W. Wen, G. Zhang, and L.-T. Hsu, "GNSS outlier mitigation via graduated non-convexity factor graph optimization," *IEEE Trans. Veh. Technol.*, vol. 71, no. 1, pp. 297–310, Jan. 2022.

[12] H. Wang, S. Pan, W. Gao, Y. Xia, and C. Ma, "Multipath/NLOS detection based on K-means clustering for GNSS/INS tightly coupled system in urban areas," *Micromachines*, vol. 13, no. 7, p. 1128, Jul. 2022.

[13] P. Axelrad, C. J. Comp, and P. F. Macdoran, "SNR-based multipath error correction for GPS differential phase," *IEEE Trans. Aerosp. Electron. Syst.*, vol. 32, no. 2, pp. 650–660, Apr. 1996.

[14] Z. Zhang, Y. Li, X. He, W. Chen, and B. Li, "A composite stochastic model considering the terrain topography for real-time GNSS monitoring in canyon environments," *J. Geodesy*, vol. 96, no. 10, pp. 79–96, Oct. 2022.

[15] F. K. Brunner, H. Hartinger, and L. Troyer, "GPS signal diffraction modelling: The stochastic SIGMA-δ model," *J. Geodesy*, vol. 73, no. 5, pp. 259–267, Jun. 1999.

[16] A. Wieser and F. K. Brunner, "An extended weight model for GPS phase observations," *Earth, Planets Space*, vol. 52, no. 10, pp. 777–782, Jun. 2014.

[17] L. Wanninger and A. Heßelbarth, "GNSS code and carrier phase observations of a Huawei P30 smartphone: Quality assessment and centimeter-accurate positioning," *GPS Solutions*, vol. 24, no. 2, Apr. 2020, Art. no. 64.

[18] Y. Li, Z. Zhang, X. He, H. Yuan, and N. Zang, "An elevation stochastic model constrained by C/N0 for GNSS real-time kinematic positioning in harsh environments," *Meas. Sci. Technol.*, vol. 34, no. 1, Jan. 2023, Art. no. 015011.

[19] P. R. R. Strode and P. D. Groves, "GNSS multipath detection using three-frequency signal-to-noise measurements," *GPS Solutions*, vol. 20, no. 3, pp. 399–412, Mar. 2015.

[20] Z. Zhang, B. Li, Y. Gao, and Y. Shen, "Real-time carrier phase multipath detection based on dual-frequency C/N0 data," *GPS Solutions*, vol. 23, no. 1, Jan. 2019, Art. no. 7, doi: 10.1007/s10291-018-0799-6.

[21] P. Špánik, L. García-Asenjo, and S. Baselga, "Optimal combination and reference functions of signal-to-noise measurements for GNSS multipath detection," *Meas. Sci. Technol.*, vol. 30, no. 4, Mar. 2019, Art. no. 044001.

[22] H. Zhou, Z. Li, C. Liu, J. Xu, S. Li, and K. Zhou, "Assessment of the performance of carrier-phase and Doppler smoothing code for low-cost GNSS receiver positioning," *Results Phys.*, vol. 19, Dec. 2020, Art. no. 103574.

[23] P. Verma, K. Hajra, P. Banerjee, and A. Bose, "Evaluating PDOP in multi-GNSS environment," *IETE J. Res.*, vol. 68, no. 3, pp. 1705–1712, Sep. 2019.

[24] R. Xi, D. Xu, W. Jiang, Q. He, X. Zhou, Q. Chen, and X. Fan, "Elimination of GNSS carrier phase diffraction error using an obstruction adaptive elevation masks determination method in a harsh observing environment," *GPS Solutions*, vol. 27, no. 3, Jun. 2023, Art. no. 139.

[25] Y. Li, Z. Zhang, X. He, Y. Wen, and X. Cao, "Realistic stochastic modeling considering the PDOP and its application in real-time GNSS point positioning under challenging environments," *Measurement*, vol. 197, Jun. 2022, Art. no. 111342.

[26] P. J. G. Teunissen, R. Odolinski, and D. Odijk, "Instantaneous BeiDou+GPS RTK positioning with high cut-off elevation angles," *J. Geodesy*, vol. 88, no. 4, pp. 335–350, Apr. 2014.

[27] D. Wujiao, "Weighting observations in combined GPS/GLONASS single point positioning based on PDOP," *J. Navig. Positioning*, vol. 1, no. 1, pp. 56–60, Jan. 2013.

[28] G. Zhang and L. Hsu, "Performance assessment of GNSS diffraction models in urban areas," *Navigation*, vol. 68, no. 2, pp. 369–389, Mar. 2021.

[29] B. Li, L. Lou, and Y. Shen, "GNSS elevation-dependent stochastic modeling and its impacts on the statistic testing," *J. Surv. Eng.*, vol. 142, no. 2, May 2016, Art. no. 04015012.

[30] M. R. Kaloop, C. O. Yigit, A. El-Mowafy, M. Bezcioglu, A. A. Dindar, and J. W. Hu, "Evaluation of multi-GNSS high-rate relative positioning for monitoring dynamic structural movements in the urban environment," *Geomatics, Natural Hazards Risk*, vol. 11, no. 1, pp. 2239–2262, Oct. 2020.

[31] R. B. Langley, "Dilution of precision," *GPS World*, vol. 10, no. 5, pp. 52–59, 1999.

[32] U.S. Space Force. (Sep. 20, 2024). *Space Segment*. [Online]. Available: https://www.gps.gov/systems/gps/space/#generations

[33] Eur. Space Agency. (Aug. 20, 2024). *Galileo IOV Satellites—Navipedia*. [Online]. Available: https://gssc.esa.int/navipedia/index.php/Galileo_IOV_Satellites

[34] Eur. Space Agency. (Aug. 20, 2024). *Galileo Future and Evolutions—Navipedia*. [Online]. Available: https://gssc.esa.int/navipedia/index.php?title=Galileo_Future_and_Evolutions

[35] Lands Dept. Hong Kong. (Aug. 20, 2024). *CORS Stations Details, Geodetic Survey of Hong Kong*. [Online]. Available: https://www.geodetic.gov.hk/en/satref/__CORS_Stations_Details.htm#hkwstchk

[36] Lands Dept. Hong Kong. (Aug. 20, 2024). *Open3Dhk*. [Online]. Available: https://3d.map.gov.hk/?l=en-US

[37] Lands Dept. Hong Kong. (Aug. 20, 2024). *Welcome To Hong Kong Satellite Positioning Reference Station Network (SatRef), Geodetic Survey of Hong Kong*. [Online]. Available: https://www.geodetic.gov.hk/en/satref/satref.htm

[38] H. Zhou, X. Wang, and S. Zhong, "A satellite orbit maneuver detection and robust multipath mitigation method for GPS coordinate time series," *Adv. Space Res.*, vol. 74, no. 6, pp. 2784–2800, Sep. 2024.

[39] D. H. Won, J. Ahn, S.-W. Lee, J. Lee, S. Sung, H.-W. Park, J.-P. Park, and Y. J. Lee, "Weighted DOP with consideration on elevation-dependent range errors of GNSS satellites," *IEEE Trans. Instrum. Meas.*, vol. 61, no. 12, pp. 3241–3250, Dec. 2012.

[40] P. J. G. Teunissen, "The least-squares ambiguity decorrelation adjustment: A method for fast GPS integer ambiguity estimation," *J. Geodesy*, vol. 70, nos. 1–2, pp. 65–82, Nov. 1995.
[41] H. Ren, G. Li, J. Geng, F. Wang, and P. Li, "Multipath hemispherical map model with geographic cut-off elevation constraints for real-time GNSS monitoring in complex environments," *GPS Solutions*, vol. 27, no. 4, Aug. 2023. Art. no. 188.
[42] H. Zhou, X. Wang, S. Zhong, Y. Li, and K. Xi, "Multipath error extraction and mitigation based on refined wavelet level and threshold selection," *GPS Solutions*, vol. 28, no. 4, Jul. 2024, Art. no. 157.
[43] H. Zhou, X. Wang, S. Li, J. Fu, X. Chen, and J. Li, "An optimal carrier-phase smoothing code algorithm for low-cost single-frequency receivers," *J. Surv. Eng.*, vol. 149, no. 4, Nov. 2023, Art. no. 05023003.
[44] S. Cheng, F. Wang, G. Li, and J. Geng, "Single-frequency multi-GNSS PPP-RTK for smartphone rapid centimeter-level positioning," *IEEE Sensors J.*, vol. 23, no. 18, pp. 21553–21561, Sep. 2023.

QINGFENG WU (Graduate Student Member, IEEE) is currently pursuing the M.Sc. degree with Shanghai Astronomical Observatory, Chinese Academy of Sciences.

His current research mainly focuses on precise GNSS data processing.

XIAOYA WANG received the Ph.D. degree from Shanghai Astronomical Observatory, Chinese Academy of Sciences, in 2001.

She has been a Professor in space geodesy data processing and applications with Shanghai Astronomical Observatory, since 2010. Her research interests include the precision orbit determination of space vehicles, TRF, EOP, and comprehensive application of GNSS/SLR/InSAR.

HOUXIANG ZHOU is currently pursuing the Ph.D. degree with the College of Surveying and Geo-Informatics, Tongji University, Shanghai, China.

His research interests focus on precise GNSS data processing and multipath error mitigation.